American Mineralogist, Volume 82, pages 497–502, 1997

Octahedral versus tetrahedral coordination of Al in synthetic micas determined by XANES

Annibale Mottana,[1] Jean-Louis Robert,[2] Augusto Marcelli,[3] Gabriele Giuli,[4] Giancarlo Della Ventura,[1] Eleonora Paris,[5] and Ziyu Wu[6]

[1]Dipartimento di Scienze Geologiche, Università di Roma Tre, Via Ostiense 169, I-00154 Roma RM, Italy
[2]Centre de Recherche sur la Synthèse et la Chimie des Minéraux, C.N.R.S., 1A rue de la Férollerie, F-45071 Orléans Cedex 2, France
[3]Laboratori Nazionali di Frascati, Istituto Nazionale di Fisica Nucleare, Via E. Fermi 13, I-00044 Frascati RM, Italy
[4]Dottorato di Ricerca in Mineralogia e Petrologia, Universita' di Firenze, Via G. La Pira 4, I-50121 Firenze, Italy
[5]Dipartimento di Scienze della Terra, Università di Camerino, Via Gentile III da Varano, I-62032 Camerino MC, Italy
[6]Institut des Matériaux de Nantes, Laboratoire de Chimie des Solides, 2 rue de la Houssinière, F-44072 Nantes Cedex 03, France

Abstract

We used the JUMBO monochromator at SSRL to measure the Al *K*-edge X-ray absorption spectra of synthetic micas having variable Al content and occupancy, from 0 to ⅔ in the octahedral M positions, and 0 to ¼ in the tetrahedral T positions. The measured Al *K* edges differ markedly, but the differences may have a common explanation: (1) Micas containing ⅓ Al in M or 1/4 Al in T have *K* edges that differ in the energy and intensity of the first two features, which are related to interaction of Al with its first-shell nearest neighbors (O and OH or F). They are nearly identical to the *K* edges of reference minerals such as albite (tetrahedral Al only) or grossular (octahedral Al only). (2) Micas containing Al in both M and T have *K* edges that can be interpreted as a weighed combination of the simple edges.

Introduction

The 2:1 layer of micas, $A(M,\square)_3[T_4O_{10}(OH,F)_2]$, consists of an octahedral sheet sandwiched between two facing tetrahedral sheets. Three bridging (''basal'') O atoms link the tetrahedral sites and form a hexagonal pattern on the outer surface of the 2:1 layer, whereas the fourth (''apical'') O atom of all tetrahedra points toward the octahedral sheet. These apical O atoms plus the OH,F anions define the octahedral sheet with three M sites per formula unit (Fig. 1). In the trioctahedral micas, all three sites are occupied by M cations, and in the dioctahedral micas only two.

Al may occupy both types of sheets: (1) in the tetrahedral sheet, where Al substitutes for Si, contributing to the net negative charge of the 2:1 layer, which is compensated by the interlayer A cation, and (2) in the octahedral sheet, where Al can occupy at most two of the three available octahedra. The three octahedra are nonequivalent with respect to their nearest-neighbor (NN) configuration (Fig. 1b): One of them (M1) has its two OH groups located at opposite corners of the octahedron, symmetrically arranged astride the mirror plane, i.e., in a ''trans'' orientation with respect to the central cation; for the remaining two sites (M2), on the contrary, the two OH groups define the common edge between two adjacent mirror-equivalent octahedra (''cis'' orientation) with all four of the O atoms lying on one side of the mirror plane.

Because of this complex crystal chemistry, micas must be investigated by a method that determines not only the Al coordination, but also the short-range order (SRO) at the T (T = Si, Be, Al) and M (M = Mg, Fe, Li, Al) sites, which complements the information on long-range order (LRO) obtained by X-ray structure refinement. So far the method of choice has been NMR (e.g., Müller et al. 1981; Herrero et al. 1985 a,b; 1987; Kinsey et al. 1985; Circone et al. 1991; Sanz and Robert 1992).

X-ray absorption near-edge structure (XANES) spectroscopy is also widely acknowledged as a local probe particularly sensitive to coordination and local environment, so that it could potentially be used to determine SRO patterns of micas (cf. Ildefonse et al. 1994). However, the Al and Si *K* edges lie in the soft X-ray range (at 1559 and 1839 eV, respectively), and because the performance inherent in XAS from the use of crystal monochromators in this energy range is believed to be poor, little work has actually been done on this matter. To our knowledge the only XANES studies of micas are nonsystematic with regard to the Al content (Brytov et al. 1979; Ildefonse et al. 1994; Li et al. 1995), or they concern atoms other than Al (e.g., Jain et al. 1980; Jagannatha Rao and Chetal 1982; Waychunas et al. 1983; Güttler et al. 1989; Cruciani et al. 1995; Heald et al. 1995).

We intend to show the usefulness of Al *K*-edge XANES spectroscopy in unravelling the coordination and elec-

0003–004X/97/0506–0497$05.00

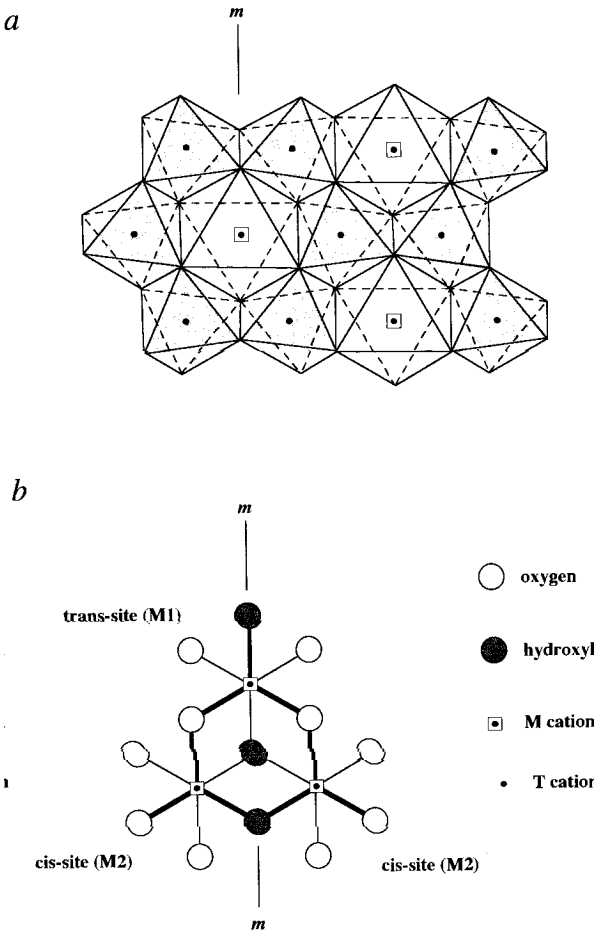

FIGURE 1. The structural environments of Al in the tetrahedral sheet (**a**) and in the octahedral sheet (**b**) of the mica structure (schematically).

tronic structure of mica sites. This paper, which is part of a more general project on end-member micas and their solid solutions, relates the results obtained for several well-characterized synthetic samples.

MATERIALS AND METHODS

Samples

Seven micas were studied; all were synthesized hydrothermally at T = 600 °C, P_{H_2O} = 2 kbar for a duration of 30 d (Table 1). All samples had been previously characterized by XRD, FTIR, Raman, and NMR spectroscopy (Robert and Kodama 1988; Robert et al. 1989; Sanz and Robert 1992), so that they can be considered as reference samples. Their compositions agree with the nominal compositions and any impurities in them are always below detection. Their crystallinity is high in spite of their very fine grain size (1 μm), as shown by the sharpness of their Bragg peaks.

Chemically these micas show a continuous trend of increasing bulk alumina content (Fig. 2). They were chosen to cover the widest possible spectrum of Al contents

TABLE 1. Synthetic micas and reference samples

Sample	Formula*
JLR1—Fluor-phlogopite	$KMg_3(Si_3Al)O_{10}F_2$
JLR2—Preiswerkite	$Na(Mg_2Al)(Si_2Al_2)O_{10}(OH)_2$
JLR4—Muscovite	$K(Al_2\square)(Si_3Al)O_{10}(OH)_2$
JLR5—Zinnwaldite (Mg)	$K(AlLiMg)(Si_3Al)O_{10}(OHF)_2$
JLR6—Polylithionite (F)	$K(Li_2Al)Si_4O_{10}F_2$
JLR7—Bityite	$Ca(Al_2Li)(Si_2AlBe)O_{10}(OH)_2$
JLR9—Ephesite	$Na(Al_2Li)(Si_2Al_2)O_{10}(OH)_2$
Grs-1—Grossular**	$Ca_{2.98}Mn_{0.01}Al_{1.97}Fe_{0.03}Si_{2.94}O_{12.00}$
Ab-4VV—albite†	$NaAlSi_3O_8$

* Idealized; Bailey 1984.
† Val Varaita, Piemonte, Italy: colorless, low-temperature hydrothermal vein in phengite micaschist, with epidote.
** Asbestos, P.Q., Canada: colorless, low-temperature hydrothermal growth on cracks in serpentinite, with chrysotile.

with their Al (1) in the tetrahedral sheet only, (2) in the octahedral sheet only, and (3) in both sheets simultaneously. In addition, they show a limited but significant spread in the type of Al nearest neighbors (F, OH, O) and next-nearest neighbors (Si and Be in T; □, Li, and Mg in M). Thus, although few in number, our sample set should permit us to make significant inferences.

We used grossular from Asbestos, Canada (Shannon and Rossman 1992), as a reference material for $^{[6]}$Al, albite from Val Varaita, Italy (Nicolas 1966) for $^{[4]}$Al, and aluminum foil was used to calibrate the energy position.

XAS Measurements

Experiments were carried out at SSRL (Stanford, CA), with the SPEAR storage ring operating at energy 3 GeV and an injection current of 100 mA. However, our experiments at room temperature were done with the operational current falling from 90 to 55 mA, so that spectra

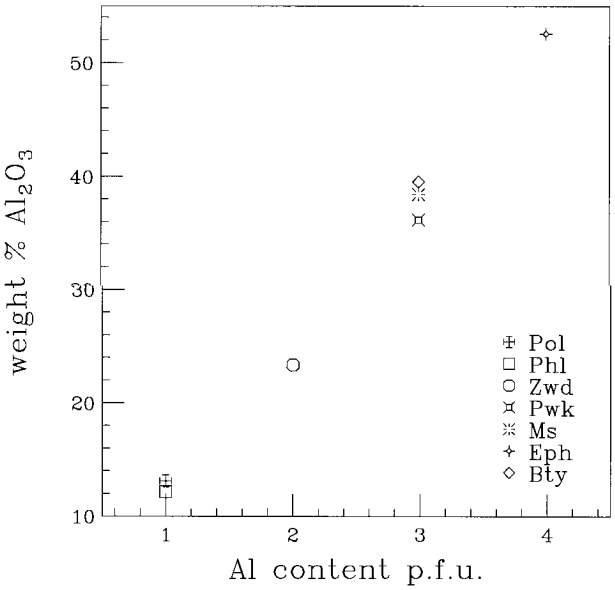

FIGURE 2. Nominal Al_2O_3 content (wt%) vs. the number of Al atoms per formula unit in the investigated synthetic micas.

had to be corrected by a simple linear normalization against standards measured at regular time intervals. We operated on beamline SB03-3, which is equipped with the JUMBO monochromator of the double-crystal type [two plates of a YB_{66} crystal cut along the (400) plane] (Rowen et al. 1993; Wong et al. 1990, 1994). Spectra were recorded in the total electron yield mode by scanning from 1540 to 1690 eV with resolution 0.46 eV at 1550 eV (M. Rowen, personal communication). Typical scan steps were 0.3–0.5 eV, and counting times 6–8 s. Details on the experimental conditions are found elsewhere (Rowen et al. 1993; Wong et al. 1994).

Samples were prepared as a homogeneous layer on a silvered, flat sample holder by allowing 3 mg of powder in 5 mL of acetone to settle gently. Being very fine grained, our micas were probably oriented flat on their cleavage plane.

Results and discussion

Experimental spectra were corrected for background contribution from lower energy absorption edges by linear fitting of the baseline and normalized in energy to +60 eV from the first inflection of the edge, i.e., at the uppermost energy value for XANES (Bianconi 1988). The spectra are given in Figure 3 and Figure 4 where they are arranged in order of increasing Al content. At first glance, there is a dramatic change in the major features of the Al *K* edge as a function not only of increasing total Al content but also of the different coordination assumed by Al in the phase.

Al in one coordination only

Polylithionite and phlogopite (Table 1) both contain one Al atom per formula unit (apfu). However, Al is located in the octahedral sheet in polylithionite (Takeda and Burnham 1969), whereas in phlogopite it is in the tetrahedral sheet (Hazen and Burnham 1973; Cruciani and Zanazzi 1994). The two minerals have XANES spectra that differ both in the energy positions of the *K* edges and in the relative intensities of the two features that constitute the main part of the edge. A simple comparison with the standards shows that the *K* edge of polylithionite (Fig. 3, Pol) is similar to that of grossular (Fig. 3, Grs), whereas the phlogopite *K* edge (Fig. 3, Phl) resembles that of albite (Fig. 3, Ab). This confirms that XANES is very sensitive to the coordination of Al in the structure.

However, each edge displays additional, characteristic, and fine features, e.g., the Al *K* edge of grossular shows at least one minor feature at 1576 eV (peak C in Fig. 3) that is absent in the edge of polylithionite. In addition there are several other features at higher energy. The smaller number of features for mica may suggest that a two-dimensional structure has a smaller number of multiple-scattering paths than the three-dimensional garnet structure. Nevertheless, given the overall similarity between the spectra, we feel safe in concluding that peaks A and B, at least, arise from identical physical effects. For grossular, Wu et al. (1996) concluded that (1) peak

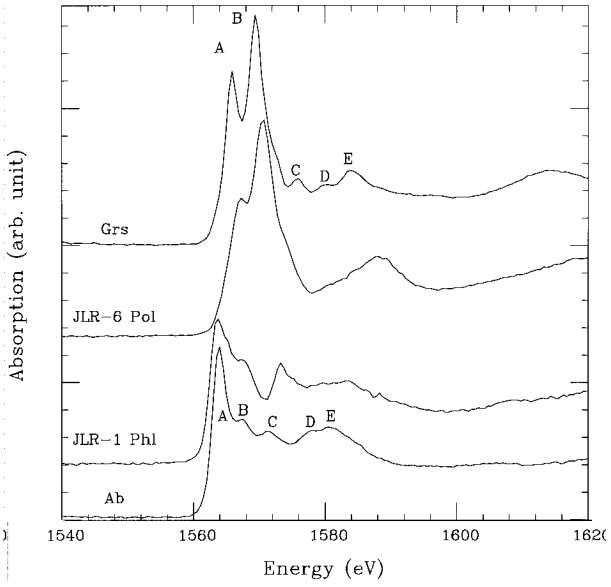

Figure 3. Experimental XANES spectra at the Al *K* edge of reference the minerals grossular (Grs) and albite (Ab) and of two synthetic micas containing either [6]Al only (polylithionite, JLR-6) or [4]Al only (phlogopite, JLR-1). See text for explanation of peak labels.

B arises from interaction of the photoelectron ejected by Al with the six O nearest neighbors that constitute the octahedral cage around the photoabsorber (i.e., they mark transitions from 1s to unoccupied p-like states) and (2) peak A is determined by the density of Al 3p empty states mixed with the empty states of the next-nearest neighbor. We believe this to be the case in polylithionite too, with the minor difference that two out of six O atoms are substituted by two OH.

The Al *K* edge of phlogopite (Fig. 3, Phl) differs from that of polylithionite in two major characteristics: (1) the negative shift in the energy position of the edge (−3 eV) and (2) the reversed intensity ratio of the two main peaks A and B. A negative shift is well-known to occur with decreasing coordination (e.g., Waychunas et al. 1983), and indeed it has been assumed to be an excellent indicator of the coordination of Al in the structure (Li et al. 1995). The reversal in the intensities of peaks A and B may be tentatively explained by analogy to the well-known fact that the 1s → 3d transition for transition metals in tetrahedral coordination produces a much stronger signal than the corresponding transition for the same metals in octahedral coordination (e.g., Bianconi et al. 1985). This conclusion is consistent with the observations for the Al *K* edge of albite (Fig. 3, Ab), in which Al is in tetrahedral coordination.

The similarity of the phlogopite and albite edges is striking, as all minor features are reproduced, even in the intermediate multiple scattering (IMS) region (1570–1590 eV). The major difference in this region is a minor shift of the phlogopite *K* edge to higher energies, which

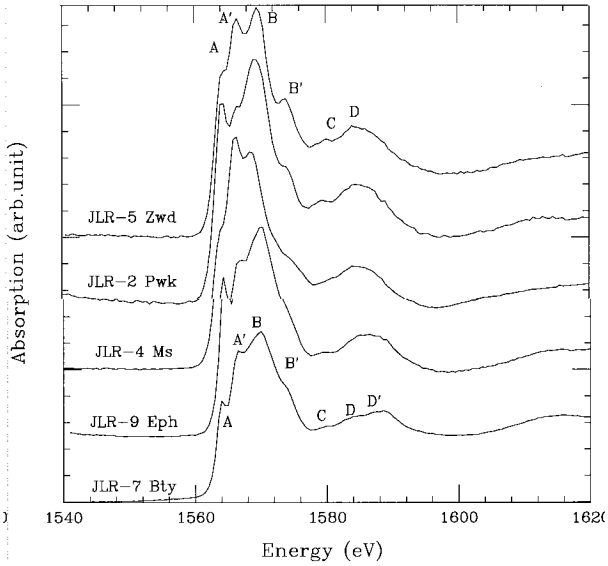

FIGURE 4. Experimental XANES spectra at the Al *K* edge of synthetic micas containing Al in two types of coordination. From top to bottom: zinnwaldite (JLR-5), preiswerkite (JLR-2), muscovite (JLR-4), ephesite (JLR-9), and bityite (JLR-7).

might be explained by a shorter distance between Al and its four O neighbors. Moreover, Al substitution within the tetrahedral sheet is disordered in our synthetic phlogopite, whereas it is strictly ordered in the framework structure of our natural low-temperature albite; this should result in a greater spread of the Al-O distances. Another detectable difference is found in the intensities. The phlogopite spectrum displays a fairly strong and sharp peak at 1574 eV (peak C), whereas the albite one has only a wider peak at lower energy (1572 eV). We assign this rather strong peak of phlogopite to an interaction of the photoelectrons ejected from Al with Si, the second-nearest neighbor of Al in the tetrahedral sheet lying on the same plane. This implies, by inference, that a peak located at ca. 1572–1575 eV is an indicator of the Si-Al ordering within the plane.

Al in tetrahedral and octahedral coordination

Figure 4 shows the XANES spectra for micas having two types of Al coordination (i.e., $^{[4]}$Al and $^{[6]}$Al) in their structure (Table 1). Zinnwaldite is the simplest case (1 Al in T + 1 Al in M: Guggenheim and Bailey 1977). The Al *K*-edge spectrum (Fig. 4, Zwd) is a weighted combination of those of phlogopite and polylithionite. The shoulder labelled A on the rising limb of the edge has the same energy as peak A in phlogopite (compare with albite), whereas peak A′, the first maximum of the edge, is in the position of peak A in polylithionite (compare with grossular). The main edge maximum, B, matches peak B in polylithionite and is the most intense feature of the spectrum, as indeed peak B is in polylithionite. Furthermore, the shoulder on its declining slope (B′) probably has the same origin as peak C in albite, and the two following features, C and D, also match peaks D and E in albite.

Preiswerkite (Fig. 4, Pwk) contains one Al in the octahedral sheet and two Al in the tetrahedral sheets of its 2:1 layer (Oberti et al. 1993). Peak A for $^{[4]}$Al, which in zinnwaldite is present as a shoulder, is a definite, well-resolved peak in preiswerkite. In contrast, peak A′, which we assigned to $^{[6]}$Al, is so weak as to be barely recognizable in the valley separating the first contribution to the edge from the edge maximum. The edge maximum itself consists of the very intense B peak, which is due to $^{[6]}$Al, and is followed on the descending limb by a weak feature B′, which is probably equivalent to B′ in zinnwaldite.

Muscovite (Fig. 4, Ms), which contains two $^{[6]}$Al and one $^{[4]}$Al (Güven 1971), has a rather sharp XANES spectrum, whose features, as expected, are the reverse of those in preiswerkite. The feature A is now weak, while A′ has higher intensity and is now the edge maximum. In contrast, features B and B′ are decidedly smaller in relation with the lower amount of Al in T. Feature C has disappeared, while D and the following features in the IMS region become even broader.

Finally ephesite (Fig. 4, Eph), which contains two $^{[6]}$Al + two $^{[4]}$Al (Slade et al. 1987), has a spectrum that resembles that of preiswerkite, however, peak A for $^{[4]}$Al is stronger and much better resolved, while peak B for $^{[6]}$Al is unusually strong, possibly because it also envelops the contribution that produced peak B′ in preiswerkite. Note that the IMS region of the ephesite spectrum is one of the best resolved among all micas examined, indicating a higher degree of local order, in agreement also with its brittle mica structure.

Next nearest neighbor effects

Muscovite and bityite both contain two Al in M and one Al in T, yet they show different Al *K*-edge XANES spectra, at least at first glance. On closer examination, however, the two spectra have identical energy positions of their features, but differ enormously in their intensities. In bityite (Lin and Guggenheim 1983), the spectrum (Fig. 4, Bty) shows the signal of the single $^{[4]}$Al as the shoulder A on the rising limb of the edge and the signals of the two $^{[6]}$Al as the second shoulder (A′) on the edge maximum (B), which is followed on its descending limb by shoulder B′. Thus, all features already recognized in muscovite are present, and most of the difference (except for the intensities) is in the IMS region, where bityite exhibits a greater number of features than muscovite.

A simple inspection to the mineral formulas (Table 1) explains the observed differences. In muscovite (a dioctahedral mica) the octahedral sheet contains two Al and a vacant site; in contrast, bityite is a trioctahedral brittle mica (Bailey 1984) with 2 Al plus one Li, which occupies the third octahedral site left vacant in muscovite. This configuration allows many more paths for the photoelectron ejected from $^{[6]}$Al; in turn, this results in a comparatively stronger interaction and a much better resolution, which can be easily seen in the spectrum as the config-

uration of the A and A′ features generated by the two $^{[6]}$Al. When considering the tetrahedral sheet, similar but reverse considerations apply: Any photoelectron ejected from $^{[4]}$Al would have the same number of scattering paths available, since the number of nearest neighbors to Al in the tetrahedral sheet is the same; however, the photoelectron has the probability of interacting with only two Si atoms, the third one having been replaced by Be. Both atoms are light, yet their scattering powers are considerably different, that of Be (Z = 4) being much lower than Si (Z = 14). Consequently, the signal contributing to the whole spectrum that arises from $^{[4]}$Al is small with respect to that arising from $^{[6]}$Al, whereas the increased number of scattering paths causes a greater number of resolved features in the intermediate scattering region.

The present results apply to synthetic disordered micas with end-member compositions, and as such they can be interpreted readily. The results cannot be extrapolated to natural micas, which exhibit significant ordering (e.g., Amisano-Canesi et al. 1994). A large collection of spectra on well-characterized materials should be obtained.

Acknowledgments

We thank the Stanford Synchrotron Radiation Laboratory (SSRL), which is supported by the Department of Energy, Office of Basic Energy Sciences and operated by Stanford University. We thank Michael Rowen, Joe Wong, and the entire technical staff for their patient assistance. The Italian M.U.R.S.T. supports our research through grants related to Project ''Cristallochimica e termodinamica'' and the European Community through a grant from Human Capital & Mobility Programme ''Access to Large Facilities.'' Reviewing by Philippe Ildefonse and an anonymous referee significantly improved the final manuscript.

References cited

Amisano-Canesi, A., Chiari, G., Ferraris, G., Ivaldi, G., and Soboleva, S.V. (1994) Muscovite- and phengite-3*T*: crystal structure and conditions of formation. European Journal of Mineralogy, 6, 489–496.

Bailey, S.W. (1984) Classification and structures of the micas. In S.W. Bailey, Ed., Micas. Mineralogical Society of America Reviews in Mineralogy, 13, 1–12.

Bianconi, A., Fritsch, E., Calas, G., and Petiau, J. (1985) X-ray absorption near-edge structure of 3d transition elements in tetrahedral coordination. The effect of bond-length variation. Physical Review B, 32, 4292–4295.

Bianconi, A. (1988) XANES spectroscopy, In D.C. Koningsberger and R. Prins, Eds., X-ray Absorption: Principles, Applications, Techniques of EXAFS, SEXAFS and XANES, p. 573–662. Wiley, New York.

Brytov, I.A., Konashenok, K.I., and Romashchenko, Yu.N. (1979) Crystallochemical effects of Al*K* and Si*K* emission and absorption spectra for silicate and aluminosilicate minerals. Geochemistry International, 16, 142–154.

Cabaret, D., Sainctavit, P., Ildefonse, P., and Flank, A.-M. (1996) Full multiple-scattering calculations on silicates and oxides at the Al K edge. Journal of Physics: Condensed Matter, 8, 3691–3704.

Circone, S., Navrotsky, A., Kirkpatrick, R.J., and Graham, C.M. (1991) Substitution of $^{[6,4]}$Al in phlogopite: Mica characterization, unit-cell variation, ^{27}Al and ^{29}Si MAS-NMR spectroscopy, and Al-Si distribution in the tetrahedral sheet. American Mineralogist, 76, 1485–1501.

Cruciani, G. and Zanazzi, P.F. (1994) Cation partitioning and substitution mechanisms in 1*M* phlogopite: A crystal chemical study. American Mineralogist, 79, 289–301.

Cruciani, G., Zanazzi, P.F., and Quartieri, S. (1995) Tetrahedral ferric iron in phlogopite: XANES and mössbauer compared to single-crystal X-ray data. European Journal of Mineralogy, 7, 255–265.

Guggenheim, S. and Bailey, S.W. (1977) The refinement of zinnwaldite-1*M* in subgroup symmetry. American Mineralogist, 62, 1158–1167.

Güttler, B., Niemann, W., and Redfern, S.A.T. (1989) EXAFS and XANES spectroscopy study of the oxidation and deprotonation of biotite. Mineralogical Magazine, 53, 591–602.

Güven, N. (1971) The crystal structure of $2M_1$ phengite and $2M_1$ muscovite. Zeitschrift für Kristallographie, 134, 196–212.

Hazen, R.M. and Burnham, C.W. (1973) The crystal structures of one-layer phlogopite and annite. American Mineralogist, 58, 889–900.

Heald, S.M., Amonette, J.E., Turner, G.D., and Scott, A.D. (1995) An XAFS study of the oxidation of structural iron in biotite mica by solutions containing Br_2 or H_2O_2. Physica B, 208–209, 604–606.

Herrero, C.P., Sanz, J., and Serratosa, J.M. (1985a) Si,Al distribution in micas: analysis by high-resolution ^{29}Si NMR spectroscopy. Journal of Physics C: Solid State Physics, 18, 13–22.

Herrero, C.P., Sanz, J., and Serratosa, J.M. (1985b) Tetrahedral cation ordering in layer silicates by ^{29}Si NMR spectroscopy. Solid State Communications, 53, 151–154.

Herrero, C.P., Gregorkiewitz, M., Sanz, J., and Serratosa, J.M. (1987) ^{29}Si MAS-NMR spectroscopy of mica-type silicates: observed and predicted distribution of tetrahedral Al-Si. Physics and Chemistry of Minerals, 15, 84–90.

Ildefonse, P., Kirkpatrick, R.J., Montez, B., Calas, G., Flank, A.-M., and Lagarde, P. (1994) ^{27}Al MAS NMR and aluminum X-ray absorption near edge structure of imogolite and allophanes. Clays and Clay Minerals, 42, 276–287.

Jagannatha Rao, B. and Chetal, A.R. (1982) An X-ray *K*-absorption study of muscovite mica. Journal of Physics D: Applied Physics, 15, L195–L197.

Jain, D.C., Usha Chandra, Garg, K.B., and Sharma, B.K. (1980) X-ray absorption study of some iron rich micas. Journal of Physics D: Applied Physics, 13, 1113–1120.

Kinsey, R.A., Kirkpatrick, R.J., Hower, J., Smith, K.A., and Oldfield, E. (1985) High resolution aluminum-27 and silicon-29 nuclear magnetic resonance spectroscopic study of layer silicates, including clay minerals. American Mineralogist, 70, 537–548.

Li, D., Bancroft, G.M., Fleet, M.E., Feng, X.H., and Pan, Y. (1995) Al *K*-edge XANES spectra of aluminosilicate minerals. American Mineralogist, 80, 432–440.

Lin, J.-C. and Guggenheim, S. (1983) The crystal structure of a Li,Be-rich brittle mica: a dioctahedral-trioctahedral intermediate. American Mineralogist, 68, 130–142.

McKeown, D.A. (1989) Aluminum X-ray absorption near-edge spectra of some oxide minerals: calculations versus experimental data. Physics and Chemistry of Minerals, 16, 678–683.

Müller, D., Gessner, W., Behrens, H.-J., and Scheler, G. (1981) Determination of the aluminium coordination in aluminium-oxygen compounds by solid-state high-resolution ^{27}Al NMR. Chemical Physics Letters, 79, 59–62.

Natoli, C.R., Benfatto, M., Brouder, C., Ruiz Lopez, M.Z., and Foulis, D.L. (1990) Multichannel multiple-scattering theory with general potentials. Physical Review B, 42, 1944–1968.

Nicolas, A. (1966) Le complexe Ophiolites-Schistes lustrés entre Dora Maira et Grand Paradis (Alpes piémontaises). Tectonique et métamorphisme. Ph.D. Thesis, University of Nantes.

Oberti, R., Ungaretti, L., Tlili, A., Smith, D.C., and Robert, J.-L. (1993) The crystal structure of preiswerkite. American Mineralogist, 78,1290–1298.

Robert, J.-L. and Kodama, H. (1988) Generalization of the correlation between OH-stretching wavenumbers and the composition of micas in the system K_2O-MgO-Al_2O_3-SiO_2-H_2O: a single model for trioctahedral and dioctahedral micas. American Journal of Sciences, 288-A, 196–212.

Robert, J.-L., Bény, J.-M., Bény, C., and Volfinger, M. (1989) Characterization of lepidolites by Raman and infrared spectrometries. I. Relationship between OH-stretching wavenumbers and composition. Canadian Mineralogist, 27, 225–235.

Rowen, M., Rek, Z.U., Wong, J., Tanaka, T., George, G.N., Pickering, I.J., Via, G.H., and Brown, G.E., Jr. (1993) First XAFS spectra with a YB_{66} monochromator. Synchrotron Radiation News, 6(3), 25–27.

Sanz, J. and Robert, J.-L. (1992) Influence of structural factors on ^{29}Si and

^{27}Al NMR chemical shifts of phyllosilicates 2:1. Physics and Chemistry of Minerals, 19, 39–45.

Shannon, R.D. and Rossman, G.R. (1992) Dielectric constants of silicate garnets and the oxide additivity rule. American Mineralogist, 77, 94–100.

Slade, P.G., Schultz, P.K., and Dean, C. (1987) Refinement of the ephesite structure in *C*1 symmetry. Neues Jahrbuch für Mineralogie Monatshefte, 275–287.

Takeda, H. and Burnham, C.W. (1969) Fluor-polylithionite: a lithium mica with nearly hexagonal $(Si_2O_5)^{2-}$ ring. Mineralogical Journal (Japan), 6, 102–109.

Waychunas, G.A., Apted, M.J., and Brown, G.E., Jr. (1983) X-ray *K*-edge absorption spectra of Fe minerals and model compounds: near-edge structure. Physics and Chemistry of Minerals, 10, 1–9.

Wong, J., Shimkaveg, G., Goldstein, W., Eckart, M., Tanaka, T., Rek, Z.U., and Tompkins, H. (1990) YB_{66}: a new soft-X-ray monochromator for synchrotron radiation. Nuclear Instruments and Methods in Physical Research, A 291, 243–249.

Wong, J., George, G.N., Pickering, I.J, Rek, Z.U., Rowen, M., Tanaka, T., Via, G.H., De Vries, B., Vaughan D.E.W., and Brown, G.E., Jr. (1994) New opportunity in XAFS investigation in the 1–2 keV region. Solid State Communications, 92, 559–562.

Wu, Z., Marcelli, A., Mottana, A., Giuli, G., and Paris, E. (1996) Effects of higher-coordination shells in garnets detected by XAS at the Al K-edge. Physical Review B, 54, 2976–2979.

Manuscript received June 27, 1996
Manuscript accepted January 22, 1997